JACS
JOURNAL OF THE AMERICAN CHEMICAL SOCIETY
pubs.acs.org/JACS
Article

Component-Specific Functions of Cu, Zn, and Zr in Inverse $ZnZrO_x$/Cu Catalysts for CO_2 Hydrogenation to Methanol

Yu Gao, Erfan Shahroudi, Stefan Bouts, Yonghui Fan, Yin Li, Peeranat Chaipornchalerm, Junbu Wang, Konstantin Klementiev, Nikolay Kosinov,* and Emiel J. M. Hensen*

Cite This: J. Am. Chem. Soc. 2026, 148, 7378−7387

ABSTRACT: Cu-based ternary catalysts often outperform their binary counterparts in the hydrogenation of CO_2 to methanol. Unraveling the underlying synergistic effects among multiple components remains challenging and requires comprehensive *operando* characterization. In this study, we present a detailed investigation into the synergistic Cu−Zn−Zr interactions in inverse $ZnZrO_x$/Cu catalysts, which show strong promise for enhancing the synthesis of methanol from CO_2. *In situ* X-ray diffraction revealed that ZrO_2 clusters effectively stabilize Cu nanoparticles against sintering during the H_2 reduction. *Operando* X-ray absorption spectroscopy at the Cu, Zn, and Zr *K*-edges demonstrated that the enhanced reducibility of Zn and Zr species arises from synergistic Cu−Zn−Zr interactions. Upon H_2 reduction, partially reduced ZrO_2 facilitated CO_2 adsorption and activation. Initially dispersed Zn^{2+} species were partially transformed into the CuZn alloy, which remained stable under reaction conditions. Notably, the CuZn alloy significantly enhanced the hydrogenation of key formate reaction intermediates to methanol. Moreover, Zn incorporation in Cu inhibited methanol decomposition to CO. The combined effects of efficient H_2 activation on highly dispersed metallic Cu, enhanced CO_2 activation by reduced ZrO_2 clusters, and rapid formate hydrogenation facilitated by the CuZn alloy rendered inverse $ZnZrO_x$/Cu catalysts superior in methanol formation rates as compared to inverse ZnO_x/Cu, ZrO_x/Cu catalysts, a commercial CuZnAl catalyst, and previously reported CuZnZr catalysts.

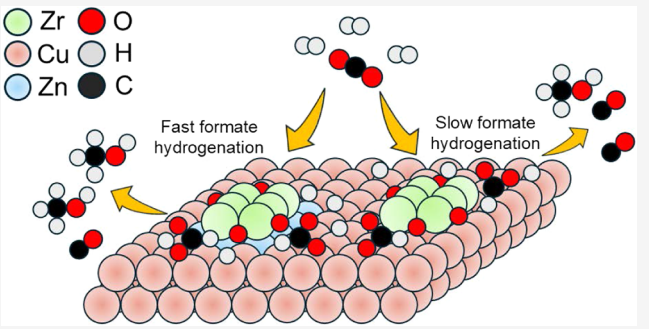

INTRODUCTION

The catalytic conversion of CO_2, a major greenhouse gas, with renewable hydrogen into chemicals is considered a promising strategy to mitigate climate change.[1] Among various products, methanol is particularly attractive due to its versatility as a platform chemical for producing a wide range of fuels and chemicals.[2] Commercial methanol synthesis is typically carried out using $Cu/ZnO/Al_2O_3$ (CuZnAl) catalysts and CO_2-containing synthesis gas (a mixture of CO and H_2) at a mild temperature (200−300 °C) and high pressure (50−100 bar). Although mechanistic studies have shown that CO_2 is the primary reactant hydrogenated to methanol over these catalysts, operating with high CO_2 concentrations introduces significant kinetic and thermodynamic challenges.[3,4] A key practical limitation is catalyst deactivation, primarily due to Cu particle sintering and oxidation at the higher H_2O pressures in the reactor.[5,6] Therefore, developing more robust and efficient catalysts for the direct hydrogenation of CO_2 to methanol remains a critical challenge.

$Cu/Zn/ZrO_2$ (CuZnZr) compositions have been recently explored as promising alternative catalysts for methanol synthesis. The stronger surface basicity of ZrO_2 compared to Al_2O_3 enhances CO_2 adsorption, while its lower hydrophilicity facilitates H_2O desorption, thereby mitigating Cu and Zn oxidation and reducing catalyst deactivation.[7,8] In addition, interfacial sites between different catalyst components can significantly influence the catalytic performance. Although pure Cu exhibits low activity for methanol synthesis,[9,10] CO_2 can be converted into formate (HCOO*) intermediates at Cu−ZrO_2 or Cu−ZnO interfacial sites, where these species are stabilized before undergoing hydrogenation to methoxy groups and ultimately methanol.[11,12] Consequently, tailoring interfacial properties represents an effective strategy to regulate the catalytic performance. One promising approach involves constructing inverse catalysts, in which oxide clusters are dispersed on metallic surfaces, thereby strengthening metal−support interactions (MSI) compared to bulk oxides.[13] Ma and coworkers showed the potential of inverse ZrO_2/Cu catalysts for CO_2 hydrogenation to methanol, reporting high methanol

Received: November 10, 2025
Revised: January 22, 2026
Accepted: January 26, 2026
Published: February 9, 2026

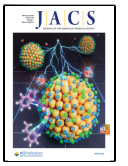

https://doi.org/10.1021/jacs.5c19915
J. Am. Chem. Soc. 2026, 148, 7378−7387

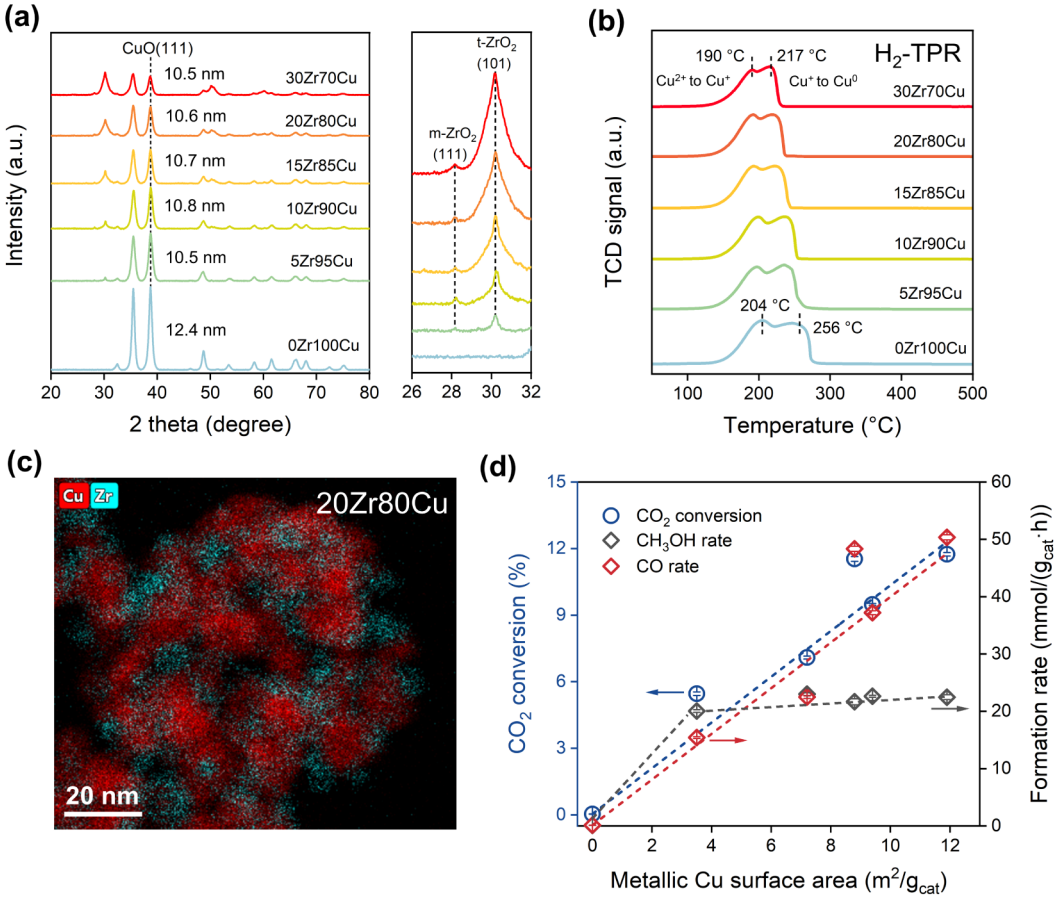

Figure 1. (a) XRD patterns of as-prepared inverse ZrO_2/Cu samples recorded at λ = 0.154 nm. The Scherrer equation was used to determine the particle sizes from the width of the CuO(111) peak; (b) H_2-TPR profiles of the inverse ZrO_2/Cu samples; (c) HAADF-STEM-EDX maps of as-prepared 20Zr80Cu; and (d) CO_2 conversion and CO and CH_3OH formation rates as a function of metallic Cu surface area (reaction conditions: $CO_2/H_2/N_2$ (10/30/10 mL/min), 50 mg of catalyst, 250 °C, and 30 bar; reaction data recorded after 12 h on stream, metallic surface areas derived from N_2O titration).

space−time−yield (STY) and promising stability.[14,15] However, a systematic investigation of inverse Cu catalysts incorporating various promoter metal oxides for methanol synthesis is still lacking.

Herein, we systematically investigated inverse Cu-based catalysts synthesized via flame spray pyrolysis (FSP) for the hydrogenation of CO_2 to methanol. Among the various promoted inverse Cu catalysts (Zr, Si, Al, Ti, Ce, Ga, and Zn), inverse ZrO_2/Cu exhibited the highest mass- and surface area-normalized CH_3OH formation rates, although with moderate CH_3OH selectivity. Inverse ZnO/Cu also exhibited promising surface area-normalized activity, together with a high CH_3OH selectivity of 86%. Building on these results, we developed inverse $ZnZrO_x$/Cu catalysts that exhibit enhanced performance in methanol synthesis, achieving a maximum methanol rate of 35.0 mmol/(g_{cat}·h) at 250 °C and 30 bar, surpassing the performance of a commercial CuZnAl catalyst. To establish structure−performance relationships in this ternary system, we employed *operando* X-ray diffraction and spectroscopy techniques. *In situ* X-ray diffraction (XRD) results revealed a strong stabilization of Cu nanoparticles by ZrO_2 clusters, with Cu particle sizes remaining unchanged during H_2 reduction. *Operando* X-ray absorption spectroscopy (XAS) data at the Cu, Zn, and Zr *K*-edges were simultaneously recorded to probe the electronic structure of the ternary Cu−Zn−Zr catalysts. The Cu species remained fully metallic throughout the H_2 reduction and CO_2 hydrogenation, serving as the primary sites for H_2 dissociation. Facile H* spillover promoted the reduction of the ZrO_2 species, thereby enhancing CO_2 activation. *In situ* IR spectroscopy revealed that the CuZn alloy, formed during H_2 reduction, markedly accelerated the hydrogenation of formate (HCOO*) intermediates to CH_3OH. This was further corroborated by formic acid (HCOOH) hydrogenation experiments, which confirmed the role of the CuZn alloy in facilitating CH_3OH formation. Additionally, incorporation of Zn was found to suppress CO formation via CH_3OH decomposition, thereby improving CH_3OH selectivity during CO_2 hydrogenation. The synergistic interplay among small metallic Cu nanoparticles, the CuZn alloy species, and reducible ZrO_2 clusters contributes to the superior performance of inverse $ZnZrO_x$/Cu catalysts in CO_2 hydrogenation to CH_3OH.

RESULTS AND DISCUSSION

ZrO_2 Promotion for CH_3OH Synthesis

A series of inverse ZrO_2/Cu samples with varying Zr content was synthesized by FSP, denoted as *x*Zr*y*Cu ($x + y = 100$; x = 0, 5, 10, 15, 20, and 30). The XRD patterns revealed characteristic diffraction lines of CuO in all as-prepared ZrO_2/Cu samples, along with diffraction lines of both tetragonal ZrO_2 (t-ZrO_2) and monoclinic ZrO_2 (m-ZrO_2) (Figure 1a).

https://doi.org/10.1021/jacs.5c19915
J. Am. Chem. Soc. 2026, 148, 7378−7387

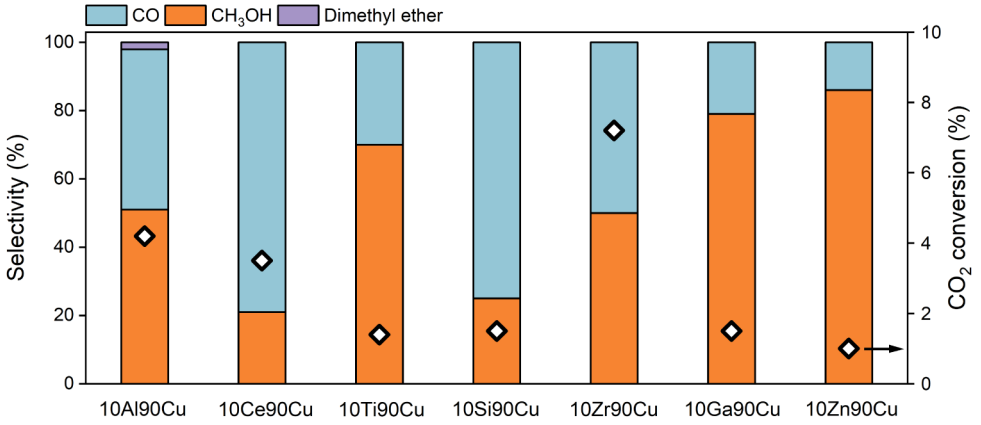

Figure 2. CO_2 hydrogenation performance over various inverse Cu catalysts (reaction conditions: $CO_2/H_2/N_2$ (10/30/10 mL/min), 50 mg of catalyst, 250 °C, and 30 bar; reaction data after 12 h on stream).

The presence of Zr in inverse ZrO_2/Cu samples led to CuO diffraction peaks that were broader than those in the FSP-prepared CuO sample, which indicates that ZrO_2 already stabilized small CuO particles during FSP synthesis. The stabilization effect extended during catalyst reduction. H_2-TPR results show that the reduction features of Cu^{2+} to Cu^+ and Cu^+ to Cu^0 shifted to lower temperatures with increasing Zr content (Figure 1b), consistent with the easier reducibility of smaller CuO nanoparticles.[16] High-resolution transmission electron microscopy (HRTEM) images and high-angle annular dark-field scanning transmission electron microscopy-energy dispersive X-ray spectroscopy (HAADF-STEM-EDX) maps for the as-prepared 20Zr80Cu sample show small ZrO_2 clusters homogeneously distributed over CuO nanoparticles (Figure 1c and Figure S1). The CO_2 hydrogenation performance of these samples was evaluated using a feed of $CO_2/H_2/N_2$ (10/30/10 mL/min) at 250 °C and 30 bar, after reduction in 20 vol % H_2 in He at 300 °C for 1 h. The inverse ZrO_2/Cu catalysts demonstrated enhanced CO_2 conversion and CO formation rate with increasing Zr content up to 20 mol %, followed by a slight decrease at a Zr content of 30 mol % (Figure S2). Notably, while the pure Cu catalyst exhibited a low CH_3OH formation rate of 0.1 mmol/(g_{cat}·h), introducing just 5 mol % Zr enhanced the rate to 20.0 mmol/(g_{cat}·h). These findings highlight that incorporating a small amount of ZrO_2 into Cu catalysts can significantly boost the CH_3OH synthesis from CO_2. The CH_3OH formation rate increased with Zr content up to 10 mol % and then leveled off. Previous studies have also shown that inverse ZrO_2/Cu catalysts exhibit significantly higher CH_3OH STY compared to conventional Cu/ZrO_2 catalysts, even when they contain comparable metallic Cu surface areas.[14,15,17] Moreover, inverse ZrO_2/Cu catalysts displayed higher CH_3OH selectivity than conventional Cu/ZrO_2 catalysts at equivalent CO_2 conversions. This improvement is attributed to the distinct interfacial sites formed between Cu nanoparticles and ZrO_2 clusters in the inverse configuration.[17] Further studies revealed that both CO_2 conversion and CO formation rates scale with the metallic Cu surface area, as determined by N_2O titration at 50 °C, across the inverse ZrO_2/Cu catalysts (Figure 1d, Figure S3, and Table S1). In contrast, the CH_3OH formation rate shows only a weak dependence on the Cu surface area. Similar trends were observed when normalizing the activity to the total specific surface area measured by N_2 physisorption (Figure S6 and Table S1). Notably, the 5Zr95Cu catalyst, despite its relatively low Cu surface area and CO_2 conversion, achieves a CH_3OH formation rate comparable to that of catalysts with higher CO_2 conversions. These findings suggest that CH_3OH synthesis is not strictly governed by Cu surface area but is likely associated with Cu−ZrO_2 interfacial sites.[15,17] Increasing Zr content beyond 5 mol % enhances Cu surface area, CO_2 conversion, and CO formation rate but does not appreciably improve CH_3OH formation, indicating saturation of the beneficial Cu−ZrO_2 interfacial sites.[15] This saturation promotes CO formation via the reverse water−gas shift (RWGS) reaction, resulting in a decline in CH_3OH selectivity with increasing CO_2 conversion (Figure S2). On the other hand, the decreased CH_3OH selectivity at higher CO_2 conversions may also result from CH_3OH decomposition.[18]

The structural and chemical promotion of ZrO_2 clusters on the hydrogenation of CO_2 to CH_3OH over Cu nanoparticles motivated the exploration of other compositions, particularly those exhibiting high CH_3OH selectivity. Accordingly, a series of inverse Cu samples comprising 10 mol % of promoters (Al, Ce, Ti, Si, Ga, and Zn) and 90 mol % Cu were synthesized by FSP. The samples are denoted 10x90Cu, where x represents the promoter. Among the prepared samples, 10Zr90Cu exhibited the highest CO_2 conversion and CH_3OH formation rate (Figures 2 and S7). Notably, 10Zn90Cu demonstrated the highest CH_3OH selectivity of 86%, indicating that Zn promotion favors CH_3OH formation over CO,[19] albeit at a lower CO_2 conversion rate. However, this catalyst showed continuous deactivation during a 12 h stability test (Figure S8), indicating that Zn is ineffective in stabilizing Cu nanoparticles against sintering. In contrast, 10Zr90Cu was stable during similar stability test. As metallic Cu dominates in reduced inverse catalysts, the specific surface area after H_2 reduction was used as an approximate measure of the active surface area (Figure S6 and Table S1). When normalized to the specific surface area, 10Zn90Cu demonstrated the second-highest CH_3OH formation rate after 10Zr90Cu (Figure S7). These findings underscore the promise of 10Zr90Cu and 10Zn90Cu for CH_3OH synthesis, with the former increasing the level of CO_2 conversion and the latter improving the CH_3OH selectivity. Notably, N_2O titration revealed a negligible metallic Cu surface area in 10Zn90Cu after H_2 reduction (Figure S4 and Table S1), indicating that Zn species covered the surface.

https://doi.org/10.1021/jacs.5c19915
J. Am. Chem. Soc. 2026, 148, 7378−7387

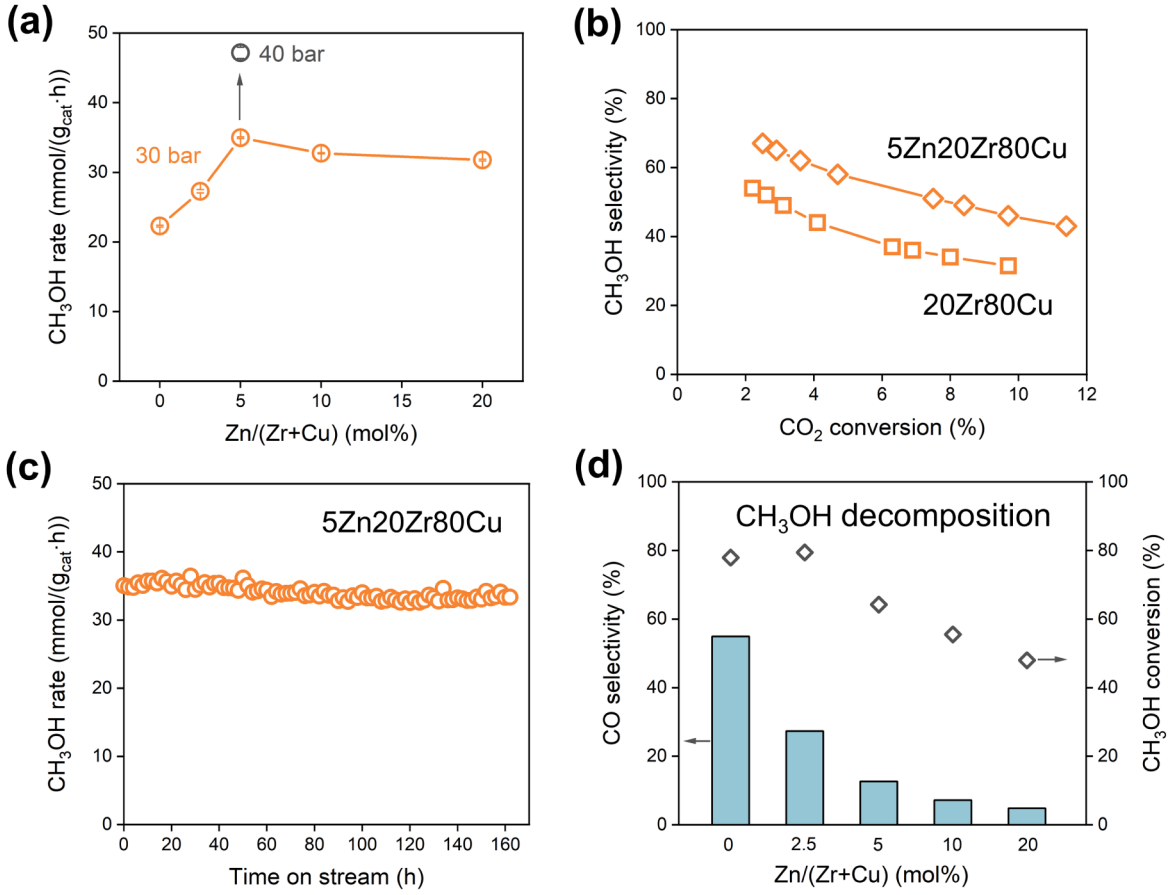

Figure 3. (a) CH_3OH formation rate of inverse $ZnZrO_x$/Cu catalysts during CO_2 hydrogenation (reaction conditions: $CO_2/H_2/N_2$ (10/30/10 mL/min), 50 mg catalyst, 250 °C, 30 bar; reaction data after 12 h on stream); (b) CH_3OH selectivity as a function of CO_2 conversion for 20Zr80Cu and 5Zn20Zr80Cu. The results were obtained by changing the contact time between the catalyst bed and reactants; (c) stability test of 5Zn20Zr80Cu during CO_2 hydrogenation; and (d) CH_3OH conversion and CO selectivity of inverse $ZnZrO_x$/Cu catalysts during CH_3OH decomposition (reaction conditions: 2 vol % CH_3OH in He (50 mL/min), 30 mg catalyst, 250 °C, and 1 bar; reaction data recorded after 3 h on stream).

Inverse $ZnZrO_x$/Cu Catalysts

Based on the observed potential of ZrO_2 for enhancing CO_2 conversion and ZnO for improving CH_3OH selectivity, both promoters were combined to further enhance CH_3OH synthesis by CO_2 hydrogenation. Starting from the most active 20Zr80Cu sample, a series of inverse $ZnZrO_x$/Cu samples with varying Zn content (i.e., Zn/(Zr + Cu) ratios of 0.025, 0.05, 0.10, and 0.2) were prepared by FSP and denoted as *x*Zn20Zr80Cu (*x* = 2.5, 5, 10, and 20). XRD patterns revealed that the CuO particles became smaller with increasing Zn content, confirming the stabilizing effect of Zn species on CuO (Figure S9). Notably, Zn species remained highly dispersed even at a high Zn content of 10 mol %, as indicated by the absence of ZnO diffraction lines. X-ray photoelectron spectroscopy (XPS) results revealed that the surface atomic Cu/Zn ratio in inverse $ZnZrO_x$/Cu samples is 2−4 times higher than that in the bulk (Figure S10 and Table S2). The high dispersion of Zn species in the inverse $ZnZrO_x$/Cu catalyst was further supported by HAADF-STEM-EDX maps (Figure S11). Spatial Pearson correlation coefficients derived from EDX pixel maps consistently showed stronger Cu−Zn than Zn−Zr proximity across all as-prepared inverse $ZnZrO_x$/Cu samples (Figure S12 and Table S3), suggesting that Zn preferentially decorates the CuO surface. Cu−Zn interactions were evident from H_2-TPR profiles (Figure S13),[20] where the reduction feature of Cu^{2+} to Cu^+ became less pronounced and the Cu^+ to Cu^0 peak shifted to higher temperatures with increasing Zn content. The CO_2 hydrogenation performance of inverse $ZnZrO_x$/Cu catalysts demonstrated an initial increase in the CH_3OH formation rate with increasing Zn content, with 5Zn20Zr80Cu exhibiting the highest rate of 35.0 mmol/(g_{cat}·h), followed by a slight decrease for 10Zn20Zr80Cu and 20Zn20Zr80Cu (Figure 3a). Under the applied reaction conditions, 5Zn20Zr80Cu also showed a CH_3OH rate higher than that of a commercial CuZnAl catalyst (31.7 mmol/(g_{cat}·h)). Moreover, it outperformed most state-of-the-art catalysts reported in the literature (Figure S14 and Table S4). The substantial improvement in CH_3OH selectivity upon Zn promotion is illustrated in Figure 3b. It was established that Zn promotion in 5Zn20Zr80Cu enhanced CH_3OH selectivity relative to 20Zr80Cu at the same CO_2 conversion: at 10% CO_2 conversion, CH_3OH selectivity was 47% for 5Zn20Zr80Cu and 31% for 20Zr80Cu. Moreover, 5Zn20Zr80Cu displayed stable catalytic performance during a 160 h stability test (Figure 3c). Increasing the reaction pressure to 40 bar resulted in a significant increase in the CH_3OH formation rate to 47.2 mmol/(g_{cat}·h) for the 5Zn20Zr80Cu catalyst (Figure 3a). Notably, trace amounts of methyl formate ($HCOOCH_3$) were detected during CO_2 hydrogenation for both the 20Zr80Cu and 5Zn20Zr80Cu

https://doi.org/10.1021/jacs.5c19915
J. Am. Chem. Soc. 2026, 148, 7378−7387

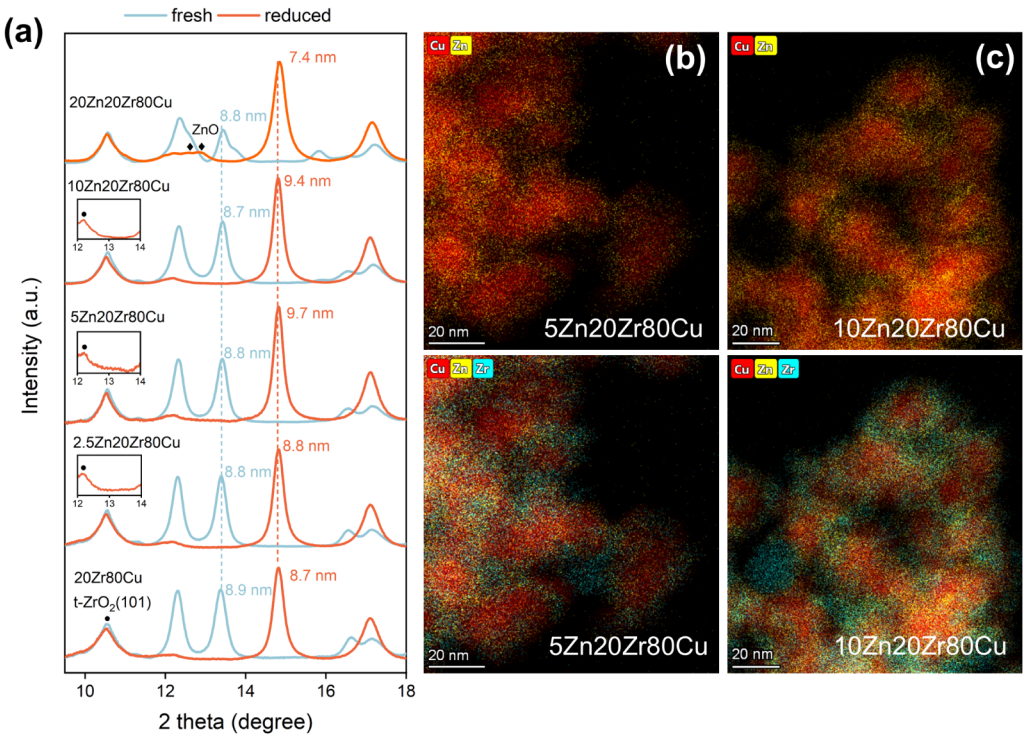

Figure 4. (a) *In situ* XRD patterns of the inverse Cu catalysts recorded at λ = 0.054 nm. The H_2 reduction was performed at 1 bar and 300 °C with a feed of H_2/He (4/16 mL/min) for 30 min, and EDX maps of (b) 5Zn20Zr80Cu and (c) 10Zn20Zr80Cu after H_2 reduction at 300 °C for 1 h. Samples were exposed to air after H_2 reduction.

catalysts (Figure S15), indicating CH_3OH decomposition.[21] CH_3OH decomposition may affect the observed CH_3OH formation rate and product distribution, as CO is the main product.[18] To investigate this, CH_3OH decomposition experiments were conducted using a feed of 2 vol % CH_3OH in He at 250 °C and 1 bar. As shown in Figure 3d and Figure S16, both CO formation rates and the CO selectivity among products such as $HCOOCH_3$, CH_4, and CO_2 were significantly suppressed by the addition of Zn, i.e., from 44.8 mmol/(g_{cat}·h) in 20Zr80Cu to 2.5 mmol/(g_{cat}·h) in 20Zn20Zr80Cu, and from 54.9% in 20Zr80Cu to 4.8% in 20Zn20Zr80Cu, respectively. This strong suppression of CH_3OH decomposition to CO by Zn incorporation contributed to the improved CH_3OH selectivity for the inverse $ZnZrO_x$/Cu catalysts during CO_2 hydrogenation (Figure 3b).

A kinetic study showed that the apparent activation energy (E_a) increased with increasing Zn content, from 57 kJ/mol for 20Zr80Cu to 81 kJ/mol for 5Zn20Zr80Cu, followed by a decrease to 60 kJ/mol for 20Zn20Zr80Cu (Figure S17). The higher E_a for inverse $ZnZrO_x$/Cu catalysts than for 20Zr80Cu is likely due to differences in the active sites. These catalysts exhibited CO_2 reaction orders between 0.10 and 0.20, suggesting strong CO_2 adsorption and high surface coverage with CO_2-derived intermediates (Figure S18). This also indicates that the role of ZrO_2 clusters in the CO_2 hydrogenation reaction relates to CO_2 adsorption and activation. Moreover, the catalysts exhibited comparable H_2 reaction orders of 0.40−0.55 (Figure S18), suggesting that Zn incorporation did not significantly promote H_2 activation. This is further supported by H_2−D_2 exchange measurements, where both 20Zr80Cu and inverse $ZnZrO_x$/Cu catalysts exhibited a similar onset temperature of HD formation at ∼120 °C (Figures S19 and S20). In contrast, a $ZnZrO_x$ catalyst showed activity only in HD at ∼235 °C, indicating that H_2 activation predominantly occurs on metallic Cu sites. Previous studies by Burch et al. have highlighted the role of ZnO in facilitating H* spillover via surface hydrides or hydroxyls in Cu/ZnO catalysts for CH_3OH synthesis.[22−24] The apparent absence of an enhanced H* spillover in inverse $ZnZrO_x$/Cu catalysts is likely due to the formation of distinct Zn-containing active sites.

Active Sites for CH_3OH Synthesis

We used *in situ* synchrotron XRD and *operando* XAS to characterize the active phase in inverse $ZnZrO_x$/Cu catalysts. The metal Cu particle sizes in 20Zr80Cu and inverse $ZnZrO_x$/Cu catalysts remained nearly unchanged after H_2 reduction (Figure 4a and Figure S21). The particle sizes derived from the CuO(111) and Cu(111) diffraction peaks differed by only ∼1 nm, underscoring the strong stabilization of Cu nanoparticles promoted by ZrO_2 clusters. Although ZrO_2 nanoparticle supports can disperse Cu clusters effectively,[25,26] our results show that ZrO_2 clusters can also efficiently stabilize Cu nanoparticles. The ZrO_2 clusters in the inverse Cu catalysts demonstrated slightly smaller particle sizes after H_2 reduction (Table S5). Unlike previously reported inverse $ZnZrO_x$/Cu samples prepared by coprecipitation, which contained ZnO clusters, the FSP-prepared inverse $ZnZrO_x$/Cu samples in this study contain highly dispersed Zn.[15,27] ZnO diffraction features were absent in 2.5Zn20Zr80Cu, 5Zn20Zr80Cu, and 10Zn20Zr80Cu after H_2 reduction (Figure 4a). The enhanced Zn dispersion is further supported by the EDX maps (Figures 4b, c, and Figure S22). Additionally, high spatial Pearson correlation coefficients between both Zn−Zr and Cu−Zn pairs were determined from the EDX maps of the inverse $ZnZrO_x$/Cu catalysts after H_2 reduction (Figure S23 and Table S6). These findings suggest that the enhanced Zn dispersion in

https://doi.org/10.1021/jacs.5c19915
J. Am. Chem. Soc. 2026, 148, 7378−7387

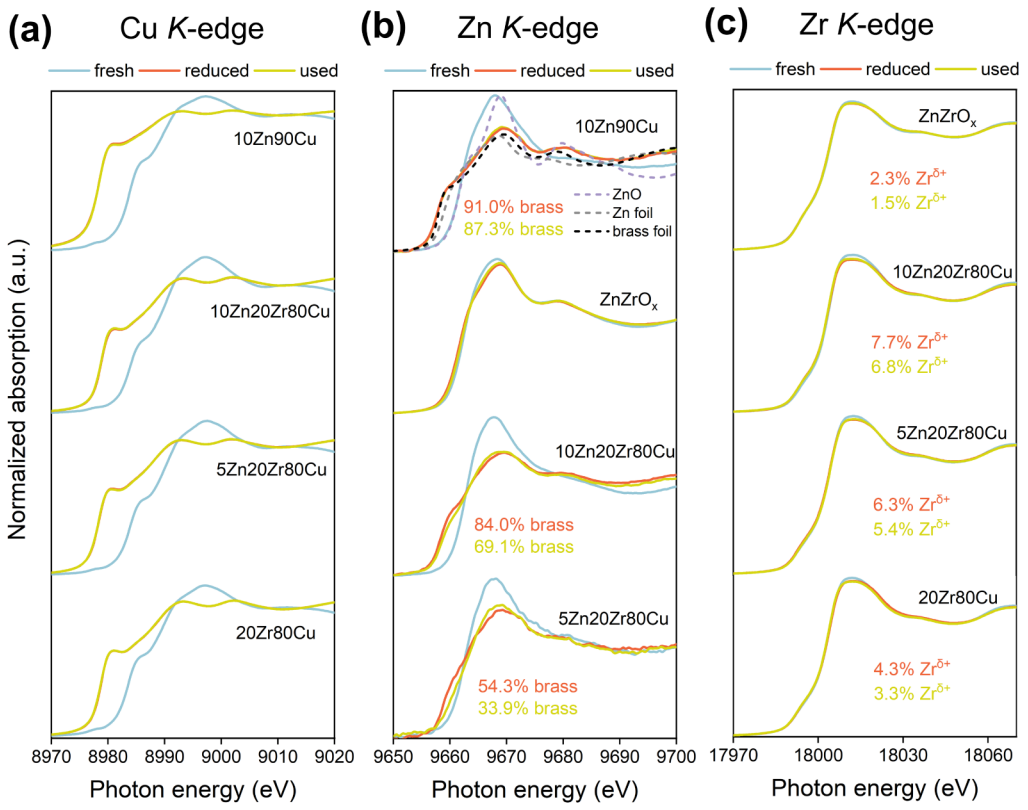

Figure 5. *Operando* (a) Cu *K*-edge; (b) Zn *K*-edge; and (c) Zr *K*-edge XANES spectra of the inverse catalysts. The H_2 reduction was performed at 300 °C with a feed of H_2/He (4/16 mL/min) for 30 min, and the CO_2 hydrogenation was performed at 250 °C and 4 bar with a feed of CO_2/H_2 (5/15 mL/min) for 20 min.

inverse $ZnZrO_x$/Cu is due to the high Cu surface area and strong Cu−Zn and Zn−Zr interactions.

Operando XAS investigations were conducted at the ROCK beamline (SOLEIL synchrotron, France),[28] where the Cu, Zn, and Zr *K*-edges XAS spectra were collected sequentially in the same experiment (Scheme S1 and Figure S24). 10Zn90Cu and $ZnZrO_x$ were used as binary references. Cu *K*-edge X-ray absorption near-edge structure (XANES) confirmed that all inverse Cu catalysts contained fully metallic Cu after H_2 reduction at 300 °C for 30 min (Figure 5a and Figures S25 to S31), consistent with the H_2-TPR results (Figure S13). The Cu species remained stable during subsequent CO_2 hydrogenation at 4 bar, as evidenced by the unchanged XANES features. Quasi-*in situ* XPS studies of the 10Zn90Cu catalyst also revealed the exclusive formation of metallic Cu species after both H_2 reduction and reaction in CO_2 hydrogenation at 6 bar for 20 h (Figure S33). Notably, 10Zn90Cu predominantly formed CuZn alloy (α-brass) upon H_2 reduction, as indicated by the Zn *K*-edge XANES (Figure 5b, Figures S26 and S34).[29−33] Given its negligible N_2O consumption after H_2 reduction (Figure S4 and Table S1), it can be concluded that N_2O did not oxidize surface CuZn alloy at 50 °C. The CuZn alloy in 10Zn90Cu also remained stable during the subsequent CO_2 hydrogenation. Zn *K*-edge XANES and LCF results confirmed the formation of CuZn alloy in inverse $ZnZrO_x$/Cu catalysts upon H_2 reduction, followed by partial dealloying during CO_2 hydrogenation (Figure 5b, Figures S28−S31). The alloy fractions during CO_2 hydrogenation were determined to be 37.7%, 33.9%, 69.1%, and 54.8% for 2.5Zn20Zr80Cu, 5Zn20Zr80Cu, 10Zn20Zr80Cu, and 20Zn20Zr80Cu, respectively (Table S7). This trend was further supported by our Zn *K*-edge k^2-weighted Fourier-transformed extended X-ray absorption fine structure (FT-EXAFS) analysis, where 10Zn20Zr80Cu displayed the highest Zn−Cu/Zn−Zn coordination numbers (Figure S34 and Table S8). XPS analysis revealed a lower surface atomic Cu/Zn ratio of 1.6 in the reduced 10Zn20Zr80Cu catalyst compared to ratios of 2.8 in the fresh catalyst (from XPS) and 8.7 in the bulk (from ICP-OES), indicating that CuZn alloy formation occurred primarily on the surface region (Figure S35). This is further supported by *in situ* XRD patterns (Figure 4a),[31] where the metallic Cu diffraction lines in reduced inverse $ZnZrO_x$/Cu catalysts show no shift relative to the 20Zr80Cu catalyst. In contrast, the $ZnZrO_x$ catalyst retained predominantly unreduced Zn species after H_2 reduction (Figure 5b and Figure S32), suggesting that metallic Cu played a crucial role in facilitating Zn reduction.[34] The redox behavior of ZrO_2 species in inverse catalysts remains underexplored in the literature, particularly using XAS. Previous *in situ* XPS studies of inverse ZrO_2/Cu catalysts have reported only a minimal shift (~0.2 eV) to lower binding energy for Zr species during H_2 reduction, a change typically within the range of experimental uncertainty, thereby rendering the actual reducibility of ZrO_2 clusters unclear.[14,35] Herein, detailed XAS investigation revealed that, compared to the $ZnZrO_x$ containing 2.3% reduced Zr species after H_2 reduction, 20Zr80Cu exhibited a higher Zr reduction degree (4.3%) (Figure 5c, Figures S27, S32, S36 and Table S7). Notably, Zn incorporation further enhanced Zr reducibility, with 7.3%, 6.3%, 7.7%, and 5.1% reduced Zr species obtained in 2.5Zn20Zr80Cu, 5Zn20Zr80Cu, 10Zn20Zr80Cu, and 20Zn20Zr80Cu, respectively (Figure 5c and Figures S28−S31). A slight reoxidation of

https://doi.org/10.1021/jacs.5c19915
J. Am. Chem. Soc. 2026, 148, 7378−7387

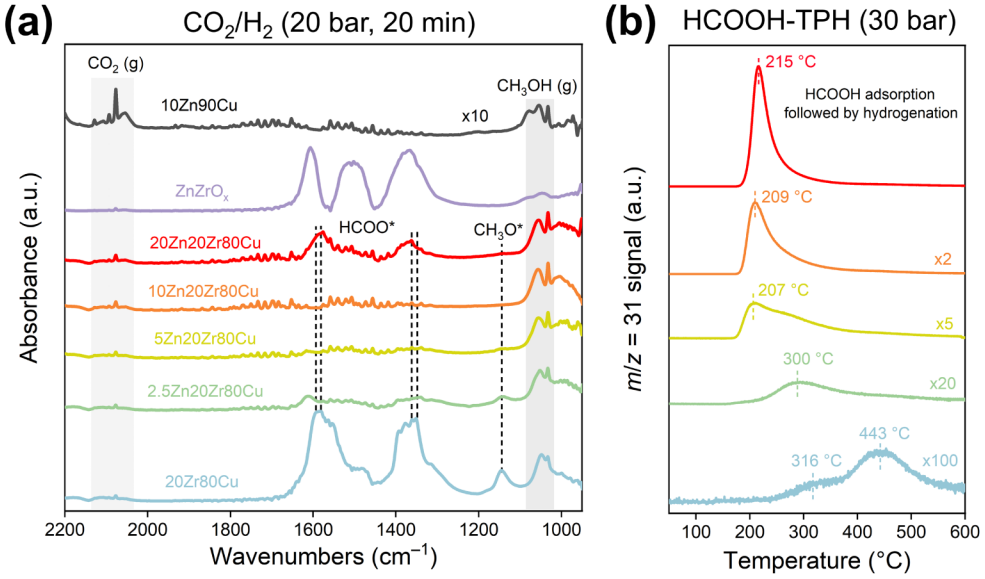

Figure 6. (a) *In situ* IR spectra of the catalysts after CO_2 hydrogenation (CO_2/H_2 = 1/3) at 250 °C and 20 bar for 20 min and (b) high-pressure HCOOH-TPH profiles of inverse Cu catalysts. Catalysts were exposed to 2 vol % HCOOH in He (50 mL/min), followed by flushing with He and then ramped from 50 to 600 °C at a rate of 5 °C/min in 20 vol % H_2 in He (50 mL/min) at 30 bar.

Zr species was observed during CO_2 hydrogenation across all Zr-containing samples, indicating the potential role of oxygen vacancies (O_v) for facilitating CO_2 adsorption and activation at the Cu−ZrO_2 interfacial sites (Figure S18).[11,36−38] These findings highlight the synergistic redox behavior among the Cu, Zn, and Zr species. The dynamic changes in the electronic properties of Zr and Zn species under different atmospheres indicate their active roles in CO_2 hydrogenation to CH_3OH.

Reaction Mechanism

To further understand the reaction pathways underlying the Zn- and Zr-promoted CH_3OH synthesis, *in situ* IR spectroscopy was performed to investigate the CO_2 hydrogenation mechanisms over inverse Cu catalysts at 250 °C and 20 bar. Formate (HCOO*) species are widely considered as the key intermediates in CH_3OH synthesis. Previous studies have identified Cu−ZrO_2 and Cu−ZnO interfacial sites as active centers for HCOO* formation.[15,39,40] As shown in Figure 6a and Figure S37, 20Zr80Cu exhibits distinct IR bands characteristic of HCOO* at 1351, 1362, 1576, and 1593 cm^{-1},[41,42] alongside signals attributed to methoxy species (CH_3O*, 1144 cm^{-1}) and gaseous CH_3OH (1030−1150 cm^{-1}).[43] Upon Zn promotion, the intensities of both HCOO* and CH_3O* features significantly decreased, becoming nearly undetectable in 2.5Zn20Zr80Cu and completely absent in 10Zn20Zr80Cu. A further increase in the Zn content in 20Zn20Zr80Cu led to a relatively small amount of HCOO*. These results suggest that Zn species accelerate the hydrogenation of HCOO* and CH_3O* species. While this effect has been observed previously in other Cu−Zn catalysts, the underlying mechanism remains poorly understood.[15,44−46] Notably, fast HCOO* hydrogenation was also observed in 10Zn90Cu but not in $ZnZrO_x$. XAS analysis reveals that CuZn alloy formation is predominant in 10Zn90Cu and also abundant in inverse $ZnZrO_x$/Cu catalysts (Figure 5b). Moreover, quasi-*in situ* XPS spectra of 10Zn90Cu after 20 h of CO_2 hydrogenation show that the CuZn alloy was preserved during the reaction (Figure S38). Based on these findings, we propose that the CuZn alloy plays a primary role in accelerating the hydrogenation of HCOO* and CH_3O*. Although CuZn alloys are frequently observed in reduced Cu−Zn catalysts, their role in CH_3OH synthesis remains debated.[40,45,47] While some studies have reported that the CuZn alloy could enhance CH_3OH formation, potentially through Zn substitution at metallic Cu step sites,[48] they are generally not considered essential for CH_3OH formation.[49−51] However, the present observation that the CuZn alloy significantly accelerates the hydrogenation of HCOO* intermediates re-emphasizes their potential importance in the reaction mechanism. This finding suggests that, although not strictly required, the CuZn alloy may play a more active and previously underappreciated role in facilitating key elementary steps in CH_3OH synthesis. Since the CuZn alloy did not promote H* spillover according to H_2−D_2 exchange results (Figure S19), it is most likely that HCOO* species formed on CuZn alloy or at CuZn alloy−ZrO_2 interfacial sites are intrinsically more active.[45] A study by Fujitani and coworkers also reported higher reactivity of HCOO* species on CuZn surfaces compared to pure Cu in model systems.[46] Nevertheless, the roles of CuZn alloy and Cu−ZnO interface in CH_3OH synthesis remain highly dependent on catalyst preparation, pretreatment, and reaction conditions.[33,52] To further investigate the HCOO* hydrogenation promoted by the CuZn alloy, we performed high-pressure HCOOH temperature-programmed hydrogenation (HCOOH-TPH) experiments on the inverse Cu catalysts. HCOO*, formed via HCOOH decomposition on the catalyst surface, can be hydrogenated into CH_3OH, providing a direct measure of the hydrogenation activity. Following H_2 reduction, the catalysts were exposed to a flow of 2 vol % HCOOH in He, then flushed with pure He, and finally heated to 600 °C at 5 °C/min in a H_2-containing atmosphere at a total pressure of 30 bar. For 20Zr80Cu, CH_3OH formation initiated at ∼250 °C, peaking at ∼443 °C (Figure 6b). The inverse $ZnZrO_x$/Cu samples exhibited much lower CH_3OH formation temperatures, with maxima at ∼300 °C for 2.5Zn20Zr80Cu, 207 °C for 5Zn20Zr80Cu, 209 °C for 10Zn20Zr80Cu, and 215 °C for 20Zn20Zr80Cu, indicating enhanced HCOOH hydrogenation

https://doi.org/10.1021/jacs.5c19915
J. Am. Chem. Soc. 2026, 148, 7378−7387

to CH_3OH upon Zn incorporation. Furthermore, the CH_3OH signal increased with Zn content, suggesting that more surface HCOOH species were converted to CH_3OH. This trend is corroborated by HCOOH temperature-programmed desorption (TPD) data, which show that more HCOOH desorbs from samples with a higher Zn content (Figure S39). Collectively, these findings demonstrate that Zn incorporation, most likely through CuZn alloy formation, substantially facilitates the hydrogenation of HCOO* intermediates. This mechanistic insight helps explain the enhanced CH_3OH formation rates observed in inverse $ZnZrO_x$/Cu during CO_2 hydrogenation.

The above discussion revealed the roles of reducible ZrO_2 clusters in stabilizing Cu nanoparticles and promoting CO_2 activation and CuZn alloy in facilitating the hydrogenation of HCOO* intermediates into CH_3OH. A schematic illustration summarizing the proposed component-specific functions of Cu, Zn, and Zr in the hydrogenation of CO_2 to CH_3OH is presented in Figure 7.

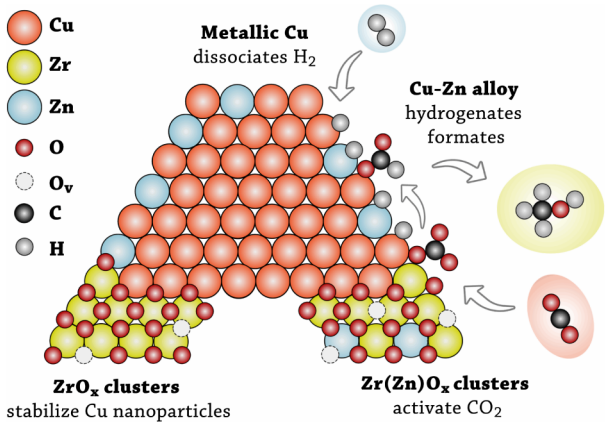

Figure 7. Schematic illustration of proposed component-specific roles of Cu, Zn, and Zr in CO_2 hydrogenation to CH_3OH.

CONCLUSION

Advanced *operando* characterization techniques are essential for uncovering complex physicochemical interactions in multicomponent catalysts under reaction conditions. In this work, we systematically elucidated the structure−performance relationships in FSP-prepared inverse $ZnZrO_x$/Cu catalysts for the hydrogenation of CO_2 to CH_3OH. *In situ* XRD revealed that ZrO_2 clusters effectively stabilize Cu nanoparticles, as evidenced by the unchanged Cu particle sizes following the H_2 reduction. *Operando* XAS at the Cu, Zn, and Zr *K*-edges demonstrated enhanced reducibility of Zr and Zn species in the inverse $ZnZrO_x$/Cu catalysts, which was attributed to synergistic interactions among Cu, Zn, and Zr. Reduced ZrO_2 species promote CO_2 adsorption and activation, assisted by H* spillover from metallic Cu, while the CuZn alloy significantly accelerates the hydrogenation of HCOO* intermediates to CH_3OH. These cooperative effects among Cu, Zn, and Zr result in superior CH_3OH synthesis rates in inverse $ZnZrO_x$/Cu catalysts compared to a commercial CuZnAl reference and all CuZnZr catalysts reported in the literature. The fundamental insights gained in this study provide a foundation for the rational design of next-generation catalysts for CO_2 hydrogenation and related sustainable chemical transformations.

ASSOCIATED CONTENT

Supporting Information

The Supporting Information is available free of charge at https://pubs.acs.org/doi/10.1021/jacs.5c19915.

Experimental methods; TEM images; ICP-OES results; N_2O titration results; N_2 physisorption results; *in situ* XRD patterns; *in situ* XPS spectra; H_2-TPR profiles; catalytic performance; H_2−D_2 exchange profiles; operando XAS results; *in situ* IR spectra; and HCOOH-TPH profiles (PDF)

AUTHOR INFORMATION

Corresponding Authors

Nikolay Kosinov − *Laboratory of Inorganic Materials and Catalysis, Department of Chemical Engineering and Chemistry, Eindhoven University of Technology, Eindhoven 5600 MB, The Netherlands;* orcid.org/0000-0001-8520-4886; Email: n.a.kosinov@tue.nl

Emiel J. M. Hensen − *Laboratory of Inorganic Materials and Catalysis, Department of Chemical Engineering and Chemistry, Eindhoven University of Technology, Eindhoven 5600 MB, The Netherlands;* orcid.org/0000-0002-9754-2417; Email: e.j.m.hensen@tue.nl

Authors

Yu Gao − *Laboratory of Inorganic Materials and Catalysis, Department of Chemical Engineering and Chemistry, Eindhoven University of Technology, Eindhoven 5600 MB, The Netherlands*

Erfan Shahroudi − *Laboratory of Inorganic Materials and Catalysis, Department of Chemical Engineering and Chemistry, Eindhoven University of Technology, Eindhoven 5600 MB, The Netherlands*

Stefan Bouts − *Laboratory of Inorganic Materials and Catalysis, Department of Chemical Engineering and Chemistry, Eindhoven University of Technology, Eindhoven 5600 MB, The Netherlands*

Yonghui Fan − *Laboratory of Inorganic Materials and Catalysis, Department of Chemical Engineering and Chemistry, Eindhoven University of Technology, Eindhoven 5600 MB, The Netherlands*

Yin Li − *Laboratory of Inorganic Materials and Catalysis, Department of Chemical Engineering and Chemistry, Eindhoven University of Technology, Eindhoven 5600 MB, The Netherlands*

Peeranat Chaipornchalerm − *Laboratory of Inorganic Materials and Catalysis, Department of Chemical Engineering and Chemistry, Eindhoven University of Technology, Eindhoven 5600 MB, The Netherlands*

Junbu Wang − *Laboratory of Inorganic Materials and Catalysis, Department of Chemical Engineering and Chemistry, Eindhoven University of Technology, Eindhoven 5600 MB, The Netherlands*

Konstantin Klementiev − *MAX IV Laboratory, Lund University, Lund SE-221 00, Sweden*

Complete contact information is available at: https://pubs.acs.org/10.1021/jacs.5c19915

Notes

The authors declare no competing financial interest.

https://doi.org/10.1021/jacs.5c19915
J. Am. Chem. Soc. 2026, 148, 7378−7387

■ ACKNOWLEDGMENTS

Yu Gao gratefully acknowledges the China Scholarship Council (CSC) for financial support. We thank Thijs Moerkens for facilitating the ICP-OES measurements and the technical assistance at the synchrotron. We also appreciate SOLEIL Synchrotron for granting proposal no. 20241129 to perform *operando* XAS experiments at the ROCK beamline, and we extend our thanks to Valérie Briois for her kind assistance. Additionally, we acknowledge the MAXIV synchrotron for proposal no. 20241189 for recording *in situ* XRD patterns at the Balder beamline, with valuable support from Mahesh Ramakrishnan, Damian Vico van Berkel, and Pietro De Angeli.

■ REFERENCES

(1) Wang, W.; Wang, S.; Ma, X.; Gong, J. Recent Advances in Catalytic Hydrogenation of Carbon Dioxide. *Chem. Soc. Rev.* **2011**, *40*, 3703−3727.
(2) Yarulina, I.; Chowdhury, A. D.; Meirer, F.; Weckhuysen, B. M.; Gascon, J. Recent Trends and Fundamental Insights in the Methanol-to-Hydrocarbons Process. *Nat. Catal.* **2018**, *1*, 398−411.
(3) Xu, D.; Wu, P.; Yang, B. Origin of CO_2 as the Main Carbon Source in Syngas-to-Methanol Process over Cu: Theoretical Evidence from a Combined DFT and Microkinetic Modeling Study. *Catal. Sci. Technol.* **2020**, *10*, 3346−3352.
(4) Shi, Y. F.; Kang, P. L.; Shang, C.; Liu, Z. P. Methanol Synthesis from CO_2/CO Mixture on Cu-Zn Catalysts from Microkinetics-Guided Machine Learning Pathway Search. *J. Am. Chem. Soc.* **2022**, *144*, 13401−13414.
(5) Kurtz, M.; Wilmer, H.; Genger, T.; Hinrichsen, O.; Muhler, M.; Cu, B. Deactivation of Supported Copper Catalysts for Methanol Synthesis. *Catal. Lett.* **2003**, *86*, 77−80.
(6) Liang, B.; Ma, J.; Su, X.; Yang, C.; Duan, H.; Zhou, H.; Deng, S.; Li, L.; Huang, Y. Investigation on Deactivation of Cu/ZnO/Al_2O_3 Catalyst for CO_2 Hydrogenation to Methanol. *Ind. Eng. Chem. Res.* **2019**, *58*, 9030−9037.
(7) Pokrovski, K.; Jung, K. T.; Bell, A. T. Investigation of CO and CO_2 Adsorption on Tetragonal and Monoclinic Zirconia. *Langmuir* **2001**, *17*, 4297−4303.
(8) Bisotti, F.; Moioli, E.; Manenti, F. Screening Kinetic Models for CO_2-to-Methanol over CuO−ZnO−ZrO_2−Al_2O_3 (CZZA) and CuO−ZnO−ZrO_2 (CZZ): Are They Consistent with the Experimental Evidence? A Critical Review of the Existing Kinetic Models and Relevant Literature on Experimental Characterization of Copper-Based Catalysts for CO_2-to-Methanol Process. *Chem. Eng. J.* **2025**, *503*, 158033.
(9) Senanayake, S. D.; Ramírez, P. J.; Waluyo, I.; Kundu, S.; Mudiyanselage, K.; Liu, Z.; Liu, Z.; Axnanda, S.; Stacchiola, D. J.; Evans, J.; Rodriguez, J. A. Hydrogenation of CO_2 to Methanol on CeO_x/Cu(111) and ZnO/Cu(111) Catalysts: Role of the Metal-Oxide Interface and Importance of Ce^{3+} Sites. *J. Phys. Chem. C* **2016**, *120*, 1778−1784.
(10) Kattel, S.; Ramírez, P. J.; Chen, J. G.; Rodriguez, J. A.; Liu, P. Active Sites for CO_2 Hydrogenation to Methanol on Cu/ZnO Catalysts. *Science* **2017**, *355*, 1296−1299.
(11) Chang, X.; Han, X.; Pan, Y.; Hao, Z.; Chen, J.; Li, M.; Lv, J.; Ma, X. Insight into the Role of Cu-ZrO_2 Interaction in Methanol Synthesis from CO_2 Hydrogenation. *Ind. Eng. Chem. Res.* **2022**, *61*, 6872−6883.
(12) Schulte, M. L.; Truttmann, V.; Doronkin, D. E.; Baumgarten, L.; Nicolai, A.; Beltran, D. A. M.; Summ, F. J.; Kiener, C.; Warmuth, L.; Pitter, S.; et al. Monitoring the Fate of Zn in the Cu/ZnO/ZrO_2 Catalyst during CO_2-to-Methanol Synthesis at High Conversions by Operando Spectroscopy. *Angew. Chem., Int. Ed.* **2025**, *64*, No. e202423281.
(13) Zhang, J.; Medlin, J. W. Catalyst Design Using an Inverse Strategy: From Mechanistic Studies on Inverted Model Catalysts to Applications of Oxide-Coated Metal Nanoparticles. *Surf. Sci. Rep.* **2018**, *73*, 117−152.
(14) Wu, C.; Lin, L.; Liu, J.; Zhang, J.; Zhang, F.; Zhou, T.; Rui, N.; Yao, S.; Deng, Y.; Yang, F.; et al. Inverse ZrO_2/Cu as a Highly Efficient Methanol Synthesis Catalyst from CO_2 Hydrogenation. *Nat. Commun.* **2020**, *11*, 5767.
(15) Xu, Y.; Wang, M.; Xie, Z.; Tian, D.; Sheng, G.; Tang, X.; Li, H.; Wu, Y.; Song, C.; Gao, X.; Yao, S.; Ma, D.; Lin, L. Insights into the Interfacial Structure of Cu/ZrO_2 Catalysts for Methanol Synthesis from CO_2 Hydrogenation: Effects of Cu-Supported Nano-ZrO_2 Inverse Interface. *Chem. Eng. J.* **2023**, *470*, 144006.
(16) Fujiwara, K.; Tada, S.; Honma, T.; Sasaki, H.; Nishijima, M.; Kikuchi, R. Influences of Particle Size and Crystallinity of Highly Loaded CuO/ZrO_2 on CO_2 Hydrogenation to Methanol. *AIChE J.* **2019**, *65*, No. e16717.
(17) Tada, S.; Fujiwara, K.; Yamamura, T.; Nishijima, M.; Uchida, S.; Kikuchi, R. Flame Spray Pyrolysis Makes Highly Loaded Cu Nanoparticles on ZrO_2 for CO_2-to-Methanol Hydrogenation. *Chem. Eng. J.* **2020**, *381*, 122750.
(18) Ortner, N.; Zhao, D.; Mena, H.; Weiß, J.; Lund, H.; Bartling, S.; Wohlrab, S.; Armbruster, U.; Kondratenko, E. V. Revealing Origins of Methanol Selectivity Loss in CO_2 Hydrogenation over CuZn-Containing Catalysts. *ACS Catal.* **2023**, *13*, 60−71.
(19) Li, J.; Wang, D.; Xiong, W.; Ding, J.; Huang, W. Interfacial Site Density Engineering of ZnO/Cu Cube Inverse Catalysts for CO_2 Hydrogenation Reactions. *ACS Catal.* **2024**, *14*, 17413−17420.
(20) Zhu, J.; Ciolca, D.; Liu, L.; Parastaev, A.; Kosinov, N.; Hensen, E. J. M. Flame Synthesis of Cu/ZnO-CeO_2 Catalysts: Synergistic Metal-Support Interactions Promote CH_3OH Selectivity in CO_2 Hydrogenation. *ACS Catal.* **2021**, *11*, 4880−4892.
(21) Ge, Y.; Gao, Z.; Xu, Y.; Xu, M.; Qin, X.; Peng, M.; Wang, S.; Gao, R.; Zhou, W.; Ma, D. Inverting Methanol Dehydrogenation Selectivity by Crowding Atomic Ni Species over α-MoC Catalysts. *Angew. Chem., Int. Ed.* **2025**, *64*, No. e202423682.
(22) Burch, R.; Golunski, S. E.; Spencer, M. S. The Role of Copper and Zinc Oxide in Methanol Synthesis Catalysts. *J. Chem. Soc., Faraday Trans.* **1990**, *1* (86), 2683−2691.
(23) Burch, R.; Golunski, S. E.; Spencer, M. S. The Role of Hydrogen in Methanol Synthesis over Copper Catalysts. *Catal. Lett.* **1990**, *5*, 55−60.
(24) Burch, R.; Chappellt, R. J.; Golunski, S. E. Synergy between Copper and Zinc Oxide during Methanol Synthesis Transfer of Activating Species. *J. Chem. Soc., Faraday Trans.1* **1989**, *85*, 3569−3578.
(25) Yu, J.; Liu, S.; Mu, X.; Yang, G.; Luo, X.; Lester, E.; Wu, T. Cu-ZrO_2 Catalysts with Highly Dispersed Cu Nanoclusters Derived from ZrO_2@ HKUST-1 Composites for the Enhanced CO_2 Hydrogenation to Methanol. *Chem. Eng. J.* **2021**, *419*, 12966.
(26) Witoon, T.; Chalorngtham, J.; Dumrongbunditkul, P.; Chareonpanich, M.; Limtrakul, J. CO_2 Hydrogenation to Methanol over Cu/ZrO_2 Catalysts: Effects of Zirconia Phases. *Chem. Eng. J.* **2016**, *293*, 327−336.
(27) Zou, T.; Araújo, T. P.; Krumeich, F.; Mondelli, C.; Pérez-Ramírez, J. ZnO-Promoted Inverse ZrO_2-Cu Catalysts for CO_2-Based Methanol Synthesis under Mild Conditions. *ACS Sustain. Chem. Eng.* **2022**, *10*, 81−90.
(28) La Fontaine, C.; Belin, S.; Barthe, L.; Roudenko, O.; Briois, V. ROCK: A Beamline Tailored for Catalysis and Energy-Related Materials from ms Time Resolution to μm Spatial Resolution. *Synchrotron Radiat. News* **2020**, *33*, 20−25.
(29) Timoshenko, J.; Jeon, H. S.; Sinev, I.; Haase, F. T.; Herzog, A.; Roldan Cuenya, B. Linking the Evolution of Catalytic Properties and Structural Changes in Copper-Zinc Nanocatalysts Using: Operando EXAFS and Neural-Networks. *Chem. Sci.* **2020**, *11*, 3727−3736.
(30) Herzog, A.; Rüscher, M.; Jeon, H. S.; Timoshenko, J.; Rettenmaier, C.; Hejral, U.; Davis, E. M.; Haase, F. T.; Kordus, D.; Kühl, S.; Frandsen, W.; Bergmann, A.; Roldan Cuenya, B. Time-Resolved Operando Insights into the Tunable Selectivity of Cu-Zn

https://doi.org/10.1021/jacs.5c19915
J. Am. Chem. Soc. 2026, 148, 7378−7387

Nanocubes during Pulsed CO_2 Electroreduction. *Energy Environ. Sci.* **2024**, *17*, 7081−7096.
(31) Zabilskiy, M.; Sushkevich, V. L.; Palagin, D.; Newton, M. A.; Krumeich, F.; van Bokhoven, J. A. The Unique Interplay between Copper and Zinc during Catalytic Carbon Dioxide Hydrogenation to Methanol. *Nat. Commun.* **2020**, *11*, 2409.
(32) Spencer, M. S. α-Brass Formation in Copper/Zinc Oxide Catalysts: I. Bulk Equilibrium Concentrations of Zinc under Methanol Synthesis and Water-Gas Shift Reaction Conditions. *Surf. Sci.* **1987**, *192*, 323−328.
(33) Beck, A.; Zabilskiy, M.; Newton, M. A.; Safonova, O.; Willinger, M. G.; van Bokhoven, J. A. Following the Structure of Copper-Zinc-Alumina across the Pressure Gap in Carbon Dioxide Hydrogenation. *Nat. Catal.* **2021**, *4*, 488−497.
(34) King, D. S.; Nix, R. M. Thermal Stability and Reducibility of ZnO and Cu/ZnO Catalysts. *J. Catal.* **1996**, *160*, 76−83.
(35) Wang, M.; Xu, Y.; Tang, H.; Tian, S.; Zeng, L.; Li, H.; Wu, C.; Hu, Z.; Su, M.; Zheng, H.; Wang, M.; Ma, D. Optimizing Methanol Synthesis from CO_2 Hydrogenation over Inverse Zr-Cu Catalyst. *Chem. Catal.* **2024**, *4*, 100985.
(36) Ro, I.; Liu, Y.; Ball, M. R.; Jackson, D. H. K.; Chada, J. P.; Sener, C.; Kuech, T. F.; Madon, R. J.; Huber, G. W.; Dumesic, J. A. Role of the Cu-ZrO_2 Interfacial Sites for Conversion of Ethanol to Ethyl Acetate and Synthesis of Methanol from CO_2 and H_2. *ACS Catal.* **2016**, *6*, 7040−7050.
(37) Fisher, I. A.; Bell, A. T. In-Situ Infrared Study of Methanol Synthesis from H_2/CO_2 over Cu/SiO_2 and $Cu/ZrO_2/SiO_2$. *J. Catal.* **1997**, *172*, 222−237.
(38) Zhang, C.; Wang, L.; Chen, Y.; He, X.; Song, Y.; Gazit, O. M.; Zhong, Z. Shifting CO_2 Hydrogenation from Producing CO to CH_3OH by Engineering Defect Structures of Cu/ZrO_2 and Cu/ZnO Catalysts. *Chem. Eng. J.* **2023**, *475*, 146102.
(39) Li, K.; Chen, J. G. CO_2 Hydrogenation to Methanol over ZrO_2-Containing Catalysts: Insights into ZrO_2 Induced Synergy. *ACS Catal.* **2019**, *9*, 7840−7861.
(40) Gómez, D.; Collins, S.; Concepción, P.; Jiménez, R.; Karelovic, A. Elucidating the Promotional Effect of Ultra-Low Zn Content on Cu for CO_2 Hydrogenation to Methanol. *J. Catal.* **2023**, *427*, 115119.
(41) Li, N.; Wang, W.; Song, L.; Wang, H.; Fu, Q.; Qu, Z. CO_2 Hydrogenation to Methanol Promoted by Cu and Metastable Tetragonal $Ce_xZr_yO_z$ Interface. *J. Energy Chem.* **2022**, *68*, 771−779.
(42) Kim, Y.; Trung, T. S. B.; Yang, S.; Kim, S.; Lee, H. Mechanism of the Surface Hydrogen Induced Conversion of CO_2 to Methanol at Cu(111) Step Sites. *ACS Catal.* **2016**, *6*, 1037−1044.
(43) Xu, Y.; Gao, Z.; Xu, Y.; Qin, X.; Tang, X.; Xie, Z.; Zhang, J.; Song, C.; Yao, S.; Zhou, W.; Ma, D.; Lin, L. Cu-Supported Nano-$ZrZnO_x$ as a Highly Active Inverse Catalyst for Low Temperature Methanol Synthesis from CO_2 Hydrogenation. *Appl. Catal., B* **2024**, *344*, 123656.
(44) Yang, M.; Yu, J.; Zimina, A.; Sarma, B. B.; Pandit, L.; Grunwaldt, J. D.; Zhang, L.; Xu, H.; Sun, J. Probing the Nature of Zinc in Copper-Zinc-Zirconium Catalysts by Operando Spectroscopies for CO_2 Hydrogenation to Methanol. *Angew. Chem., Int. Ed.* **2023**, *62*, No. e202216803.
(45) Lam, E.; Noh, G.; Larmier, K.; Safonova, O. V.; Copéret, C. CO_2 Hydrogenation on Cu-Catalysts Generated from Zn^{II} Single-Sites: Enhanced CH_3OH Selectivity Compared to $Cu/ZnO/Al_2O_3$. *J. Catal.* **2021**, *394*, 266−272.
(46) Nakamura, J.; Choi, Y.; Fujitani, T. On the Issue of the Active Site and the Role of ZnO in Cu/ZnO Methanol Synthesis Catalysts. *Top. Catal.* **2003**, *22*, 277−285.
(47) Li, M. M. J.; Zeng, Z.; Liao, F.; Hong, X.; Tsang, S. C. E. Enhanced CO_2 Hydrogenation to Methanol over CuZn Nanoalloy in Ga Modified Cu/ZnO Catalysts. *J. Catal.* **2016**, *343*, 157−167.
(48) Behrens, M.; Studt, F.; Kasatkin, I.; Kühl, S.; Hävecker, M.; Abild-Pedersen, F.; Zander, S.; Girgsdies, F.; Kurr, P.; Kniep, B.-L.; Tovar, M.; Fischer, R. W.; Nørskov, J. K.; Schlögl, R. The Active Site of Methanol Synthesis over $Cu/ZnO/Al_2O_3$ Industrial Catalysts. *Science* **2012**, *336*, 893−897.
(49) Gao, Y.; Fan, Y.; Zhang, H.; Pornsetmetakul, P.; Mezari, B.; Wagemakers, J.; Ramakrishnan, M.; Klementiev, K.; Kosinov, N.; Hensen, E. J. M. Stable CO_2 Hydrogenation to Methanol by Cu Interacting with Isolated Zn Cations in Zincosilicate CIT-6. *ACS Catal.* **2025**, *15*, 1807−1818.
(50) Zabilskiy, M.; Sushkevich, V. L.; Newton, M. A.; Van Bokhoven, J. A. Copper-Zinc Alloy-Free Synthesis of Methanol from Carbon Dioxide over Cu/ZnO/Faujasite. *ACS Catal.* **2020**, *10*, 14240−14244.
(51) Kandemir, T.; Girgsdies, F.; Hansen, T. C.; Liss, K. D.; Kasatkin, I.; Kunkes, E. L.; Wowsnick, G.; Jacobsen, N.; Schlögl, R.; Behrens, M. InSitu Study of Catalytic Processes: Neutron Diffraction of a Methanol Synthesis Catalyst at Industrially Relevant Pressure. *Angew. Chem., Int. Ed.* **2013**, *52*, 5166−5170.
(52) Choi, Y.; Futagami, K.; Fujitani, T.; Nakamura, J. The Difference in the Active Sites for CO_2 and CO Hydrogenations on Cu/ZnO-Based Methanol Synthesis Catalysts. *Catal. Lett.* **2001**, *73*, 27−31.

https://doi.org/10.1021/jacs.5c19915
J. Am. Chem. Soc. 2026, 148, 7378−7387